Research Square

Preprints are preliminary reports that have not undergone peer review.
They should not be considered conclusive, used to inform clinical practice,
or referenced by the media as validated information.

Aberrant Autophagy–Senescence Axis Drives Spontaneous Abortion through HSPA6/FOXO1-Mediated Decidual Stromal Dysfunction

Hai-Xia Tan
Obstetrics and Gynecology Hospital of Fudan University
Shao-Liang Yang
Obstetrics and Gynecology Hospital of Fudan University
Jia-Wei Shi
Shanghai Jiao Tong University
Meng-Ying Li
Obstetrics and Gynecology Hospital of Fudan University
Si-Man Chen
Obstetrics and Gynecology Hospital of Fudan University
Xiao-Yan Cao
Obstetrics and Gynecology Hospital of Fudan University
Wen-Jie Zhou
Shanghai Jiao Tong University School of Medicine
Ming-Qing Li
mqli@sjtu.edu.cn

Shanghai Jiao Tong University School of Medicine https://orcid.org/0000-0002-9276-0722
Feng Xie
Obstetrics and Gynecology Hospital of Fudan University

Research Article

Keywords: autophagy, senescence, HSPA6, FOXO1, abortion

Posted Date: July 3rd, 2026

DOI: https://doi.org/10.21203/rs.3.rs-10130007/v1

License: This work is licensed under a Creative Commons Attribution 4.0 International License.
Read Full License

Version of Record: A version of this preprint was published at Cellular and Molecular Life Sciences on November 7th, 2026. See the published version at https://doi.org/10.1007/s00018-026-06508-3.

Abstract

Abnormal senescence of decidual stromal cells is tightly linked to spontaneous abortion, yet the underlying mechanisms remain poorly defined. In this study, we found that the senescence level of DSCs in the decidual tissues of patients with recurrent spontaneous abortion (RSA) significantly increased during the first trimester. Using both *in vitro* and *in vivo* models, we show that abnormally elevated branched-chain amino acids (BCAAs) reduce autophagic flux, leading to excessive DSC senescence, which mechanistically involves aberrant heat shock protein A6 (HSPA6) upregulation and subsequent the core transcription factor forkhead box O1 (FOXO1) downregulation, thereby predisposing to adverse pregnancy outcomes. Both *in vitro* and *in vivo* experiments demonstrated that the reduced macroautophagy/autophagy flux resulting from abnormally elevated branched-chain amino acids (BCAAs) leads to excessive DSC senescence. *In vivo* studies, intervention with leucine, a key BCAA, promoted uterine senescence and induced adverse pregnancy outcomes in mice. Conversely, restoring autophagy with rapamycin effectively suppressed excessive senescence at the maternal-fetal interface and significantly improved pregnancy outcomes under high-leucine conditions. Therefore, this study demonstrates that excessive senescence at the maternal-fetal interface, resulting from impaired autophagy flux, disrupts pregnancy maintenance via the HSPA6-FOXO1 signaling pathway. These findings highlight the role of metabolic disorders and autophagy imbalance in miscarriage, and offer potential therapeutic strategies for preventing spontaneous abortion.

Introduction

Recurrent spontaneous abortion (RSA) is one of the most common complications of early pregnancy, affecting approximately 1–2% of couples[1]. Currently, the common causes of RSA include chromosomal abnormalities, immune disorders, endocrine diseases, uterine malformations, genetic lesions, and male sperm abnormalities, etc. However, about 50% of patients in clinical still have unknown causes, which are classified as unexplained recurrent spontaneous abortion (URSA) [2–4]. Due to the lack of clear cause diagnosis, these patients are unable to receive targeted treatment and often fall into a vicious cycle of repeated pregnancies and miscarriages.

Cellular senescence is a stable state of cell cycle arrest. It is no longer merely regarded as a sign of aging or degeneration, but rather plays an active and indispensable physiological regulatory role in embryo implantation and pregnancy maintenance[5, 6]. However, the accumulation of excessive senescent cells can induce an imbalance in the senescence-associated secretory phenotype (SASP) (such as IL-6, IL-1β, TNF-α, etc), triggering local chronic inflammation and disorder of the immune tolerance microenvironment, thereby destroying the homeostasis of the maternal-fetal interface and causing adverse pregnancy outcomes[7–9]. Therefore, more and more people are trying to analyze the specific roles of different SASP molecules in maternal-fetal crosstalk and exploring precision intervention strategies. Yet, distinguishing physiological from pathological senescence for targeted intervention remains a major translational challenge at this early stage.

Autophagy, a highly conserved lysosomal degradation pathway essential for maintaining cellular proteostasis and organelle integrity, plays a pivotal role in the establishment and maintenance of pregnancy[10]. Previous studies have shown that moderate autophagy activity can provide the necessary energy substrates for decidualization by degrading damaged organelles and misfolded proteins, thereby maintaining the survival and functional stability of decidual cells[11–13]. Conversely, the imbalance of autophagy (overactivation or inhibition) leads to adverse pregnancy outcomes by inducing inflammatory responses in decidual immune cells or damaging the interaction at the maternal-fetal interface[14, 15]. Notably, autophagy plays a protective role in the initial stage of cellular senescence. Its core mechanism is to clear damaged organelles and protein aggregates through selective autophagic pathways such as mitophagy and ribophagy to maintain cellular homeostasis[16–18]. However, it remains unclear how autophagy precisely governs decidual senescence and which metabolic signals serve as upstream triggers to initiate this regulatory axis.

Therefore, it is urgent to elucidate the molecular mechanisms of senescence regulation in DSCs, specifically how aberrant BCAA metabolism disrupts autophagic homeostasis as an upstream trigger to induce cellular senescence, and its pathological significance in spontaneous abortion. This work will provide novel metabolic intervention strategies and potential therapeutic targets for early pregnancy failure.

Materials and methods

Patients and samples collection

Patients were confirmed to be pregnant through ultrasound and blood tests. Decidual tissues were collected from women undergoing elective termination of pregnancy (n = 65) and patients diagnosed with RSA (n = 40). Participants were aged 21 to 38 years, with a gestational age of 7 to 9 weeks. The inclusion criteria for the control group were absence of abdominal pain, vaginal bleeding, infection, or history of adverse pregnancy outcomes. RSA was defined as the occurrence of two or more consecutive spontaneous pregnancy losses before 24 weeks of gestation, following the exclusion of known endocrine or genetic factors. All samples were collected under sterile conditions according to established diagnostic criteria. Tissues were immediately immersed in ice-cold DMEM/F-12 medium (HyClone, SH30023.01) and transported to the laboratory within 30 minutes for the isolation and primary culture of DSCs.

DSCs isolation and culture

Decidual tissues were washed in phosphate-buffered saline (PBS; HyClone, SH30256.01) and finely minced into approximately 1 mm^3 fragments. The tissue was enzymatically digested in a mixture containing 0.1% Collagenase Type IV (Sigma-Aldrich, C4-22-1G) and 5% DNA enzymes (3000 IU; Sigma-Aldrich, D5025) at 37°C for 30 min with constant agitation. Digestion was terminated by the addition of

DMEM/F-12 medium (HyClone, SH30023.01) supplemented with 10% fetal bovine serum (FBS; Thermo Fisher Scientific, A5256701). The cell suspension was filtered through sieves (mesh sizes: 100, 300 and 400) to remove undigested tissue debris, followed by centrifugation at 1300 rpm for 10 min to obtain cell particles. Subsequently, 20%, 40% and 60% Percoll (GE Healthcare Life Sciences, 17-0891-01) were prepared, and then the DSCs at the 20%-40% interface was recovered by centrifugation at 2500 rpm for 30 min. After low-speed centrifugation again, the supernatant was discarded, and the cells were resuspended in DMEM/F-12 medium containing 10% FBS. The isolated DSCs were cultured at 37°C in a humidified incubator with 5% CO_2.

Cell transfection

Recombinant lentiviruses expressing siRNA targeting HSPA6 (siHSPA6) and control lentivirus with GFP (siNC) were obtained from Genomeditech Co., Ltd. (Shanghai, China). DSC cells were seeded in 6-well plates (5×10^4 cells/ml) and when the fusion rate reached 30%, the cells were infected with siHSPA6 and its corresponding siNC. According to the manufacturer's instructions, the optimal transfection condition for MOI is that 80% of the infected cells are completed within the optimal time. The required virus volume was calculated, and the cells were replaced with fresh medium after 12 h of infection for continued culture. The infection efficiency was evaluated by GFP fluorescence intensity and post-infection RT-PCR.

Immunohistochemistry

The paraffin sections of human decidua were baked at 60°C for 2 hours, dewaxed with xylene, and then dehydrated in graded ethanol. The tissue sections underwent antigen retrieval in Tris–EDTA buffer (pH 9.0) (Solarbio, C1034) for 15 min. After cooling at room temperature for 1 h, the endogenous peroxidase was then removed with 3% hydrogen peroxide (H_2O_2) and cultured with 5% bovine serum albumin (BSA) for 1 h at room temperature. Then, the samples were incubated with rabbit anti-human CDKN2A antibody (1:100; Abcam, ab51243), rabbit anti-human CDKN1A antibody (1:100; Abcam, ab109520), and rabbit anti-human TP53 antibody (1:100; Abcam, ab32049) or Rabbit IgG, polyclonal isotype control (1:200; Abcam, ab171870) overnight in humid chamber at 4°C. After washing the sections three times with PBS, the sections were cultured and the signals were visualized using the GTvision TMIII immunohistochemical detection kit (Gene Tech, GK500710). The sections were stained with hematoxylinin (Well Biotech, WH2013).

Immunofluorescence and Immunocytochemistry

The steps were the same as above. After baking, dewaxing, dehydration, antigen repair and serum blocking, the tissue samples were incubated with rabbit anti-human/mouse CDKN2A antibody (1:100; Abcam, ab51243), rabbit anti-human CDKN1A antibody (1:100; Abcam, ab109520) and rabbit anti-mouse

CDKN1A antibody (1:100; EpiZyme, P012989), rabbit anti-human TP53 antibody (1:100; Abcam, ab32049), rabbit anti-mouse TP53 antibody (1:100; EpiZyme, P010266), rabbit anti-human/mouse FOXO1 antibody (1:100; Cell Signaling Technology, 2880T), mouse anti-human/mouse vimentin (1:4000; proteintech, 60330-1-1g), overnight in humid chamber at 4°C. After washing three times with PBS, the sections were incubated with Goat Anti-Mouse IgG H&L (Alexa Fluor® 488) preadsorbed antibody (1:500; Abcam, ab150113) and Goat Anti-Rabbit IgG H&L (Alexa Fluor® 647) preadsorbed antibody (1:500; Abcam, ab150079) for 1 h at room temperature. And the nuclei were stained with 4′,6-diamidino-2-phenylindole (DAPI; Beyotime, C1006).

Primary DSCs isolated from NP or RSA women, or DSCs treated with media containing and lacking BCAA (Livning; LVN1004-BCAA) for 96 h. Then cells were seeded in a flat-bottom 24-well plate with cover glasses at the bottom (5×10^4 cells/well). Cells were fixed with 4% paraformaldehyde, permeabilized with 0.1% Triton X-100 (Beyotime, ST795), and blocked with 5% BSA in PBS. These cells were then incubated overnight at 4°C with rabbit anti-human FOXO1 antibody (1:100; Cell Signaling Technology, 2880T) and rabbit anti-human HSPA6 antibody (1:100; EpiZyme, P107765). After washing three times with PBS, cells were incubated with Goat Anti-Rabbit IgG H&L (Alexa Fluor® 647) preadsorbed antibody (1:500; Abcam, ab150079) for 1 h at room temperature. The nuclei were stained with 4',6-diamidino-2-phenylindole (DAPI, Beyotime, C1002). All images were taken by a high-resolution fluorescence microscope Thunder (Leica).

SA-β-gal staining

Using the Cell senescence β -galactosidase staining Kit (Beyotime, C0602), the frozen sections were first thawed, and the tissues were soaked and washed three times with PBS. The sections were then fixed with β -galactosidase staining fixative for 15 min at room temperature, followed by three washes with PBS. The tissues were incubated with X-gal-containing staining working solution at 37°C for 48 h in a CO_2-free incubator. To prevent evaporative loss of the staining solution, the incubation chambers were sealed with parafilm.

For cell experiments, DSCs were seeded in 6-well plates (5×10^5 cells/well) and treated with or without BCAA medium (96 h), 3-methyladenine (3-MA; 10 mM, 48 h), or D-galactose (D-Gal; 30 mM, 48 h). After treatment, cells were washed with PBS and fixed for 15 min. Subsequent staining procedures were performed as described for the tissue sections. Images were taken by microscope (Olympus). At least three random fields were counted per well to determine the percentage of SA-β-gal-positive cells. All experiments were performed in triplicate.

Western blot

DSCs treated with BCAA for various durations (0, 2, 4, 6, 8 days); with or without BCAA medium for 96 h; 3-MA (10 mM; MedChemExpress, HY-19312) for 48 h; Rapamycin (2 μM; MedChemExpress, HY-10219) treatment for 48 h; H_2O_2 (200 μM; Sigma-Aldrich, H1009) for 24 h; or D-galactose (30 mM;

MedChemExpress, HY-N0210) for 48 h. Additionally, DSCs were transfected with siRNA targeting HSPA6 (siHSPA6) or a negative control (siNC). After treatment, cells were washed with PBS and lysed in RIPA lysis buffer (Beyotime, P0013B) supplemented with 1% phenylmethylsulfonyl fluoride (PMSF; Beyotime, ST506). After incubation on ice for 30 min, cells were scraped and centrifuged at 12,000 rpm for 30 min at 4°C. Total protein (20 μg) was transferred to a PVDF membrane (Merck Millipore, IPVH00010) by electrophoresis in 12.5% SDS-PAGE (Epizyme, PG113) for 80 min. Membranes were blocked in 5% skim milk in TBST (Tris-buffered saline [Servicebio, G0001-15] with Tween 20 [Sigma-Aldrich, 8221840500]) at room temperature for 1 h. Then, membranes were incubated overnight at 4°C with the following primary antibodies: rabbit anti-human/mouse CDKN2A (1:1000; Abcam, ab51243), rabbit anti-human CDKN1A (1:1000; Abcam, ab109520), rabbit anti-mouse CDKN1A (1:1000; Epizyme, P012989), rabbit anti-human TP53 (1:1000; Abcam, ab32049), rabbit anti-mouse TP53 (1:1000; Epizyme, P010266), rabbit anti-human MAP1LC3B (1:1000; Cell Signaling Technology, 3868T), rabbit anti-mouse MAP1LC3B (1:1000; Epizyme, R013940), rabbit anti-human/mouse SQSTM1 (1:1000; Cell Signaling Technology, 39749T), rabbit anti-human/mouse ATG5 (1:1000; Abcam, ab108327), rabbit anti-human FOXO1 (1:1000; Cell Signaling Technology, 2880T), and rabbit anti-human/mouse HSPA6 (1:1000; Epizyme, P107765). After washing three times with TBST, the membranes were incubated with HRP-conjugated goat anti-rabbit IgG (1:3000; Cell Signaling Technology, 7074S) or HRP-conjugated goat anti-mouse IgG (1:4000; Biodragon, BF03001) secondary antibodies. Finally, membranes were washed three times and processed for chemiluminescence using the Immobilon Western Chemiluminescent HRP Substrate Kit (Merck Millipore, WBKLS0100). All experiments were performed in triplicate.

Reactive oxygen species detection

Reactive oxygen species detection
Dilute DCFH-DA (Beyotime, S0034S) with probe dilutive at a ratio of 1:1000. Usually, add 1 ml of the diluted DCFH-DA to one well of a 6-well plate. Incubate in a 37 ° C cell incubator for 20 min in the dark. After incubation, the cells were washed three times with PBS to sufficiently remove extracellular DCFH-DA. The ROS levels in the cells were measured by flow cytometry.

Transcriptome sequencing

DSCs were treated with or without BCAA for 96 h, or with D-galactose (30 mM) for 48 h, followed by RNA-Seq. Total RNA was extracted according to the standard instructions, and its quality was evaluated by Agilent 2100 bioanalyzer. After the library quality inspection was qualified, sequencing libraries were constructed and sequenced on the Illumina NovaSeq platform, generating 150 bp paired-end reads. Raw data were subjected to quality control processing to remove adapter sequences, poly-N-containing reads, and low-quality reads. Clean paired-end reads were aligned to the reference genome using HISAT2 v2.0.5. Gene read counts were calculated using featureCounts, and DESeq2 software(v1.16.1) was used for gene expression normalization and differential expression analysis. Gene set enrichment analysis was conducted using the clusterProfiler R package for GO functional annotation and KEGG pathway

enrichment analysis. Differentially expressed genes (DEGs) were defined according to the following criteria: expression amount fold difference threshold |logFC| > 1; expression difference significance threshold P-value < 0.05. Additionally, protein-protein interaction (PPI) network analysis of DEGs was performed based on the STRING database, and network visualization was constructed using Cytoscape software.

Real time (RT)-PCR

Total RNA was extracted from DSCs treated with or without BCAA for 96 h, 3-MA for 48 h, rapamycin for 48 h, H_2O_2 for 24 h, or D-galactose for 48 h, as well as from decidual tissues of normal early pregnancy and RSA patients, using TRIzol® reagent (Invitrogen, 15596018) or the Total RNA Isolation Kit (NCM Biotech, M5105). Subsequently, RNA was reverse transcribed into cDNA using the PrimeScript RT reagent kit (Takara, RR036A). RT-PCR was performed with SYBR Premix Ex Taq (Takara, RR820A) on an ABI Prism 7900 Fast Sequence Detection System (Thermo Fisher Scientific). Each sample was assayed in three replicate wells and analyzed using the $2^{-\Delta\Delta Ct}$ method. The relative mRNA expression levels were normalized to GAPDH. The primer sequences of these genes are provided in Table S1.

Mice

The C57BL/6JGpt mice were purchased from Jiangsu GemPharmatech Co., Ltd. (Nanjing, China) and acclimatized for 2 weeks in SPF experimental animal facility. 8-week-old female mice were mated with 8-week-old male mice (2:1) to establish a pregnant mouse model. Pregnancy was confirmed on the day when vaginal thrombus was observed (day 0.5), and the pregnant mice were randomly divided into the control group (1.2% leucine) and the experimental group (6% high leucine), and all feeds were provided by Wuxi Fanbo Biotechnology Co., LTD. Samples were collected at 13.5 days of pregnancy. The total number of embryos, embryo absorption rate, and the weight of embryos and placentas were counted.

Pregnant mice were randomly divided into a control group and an experimental group, both of which were fed 6% high-leucine. The experimental group received intraperitoneal injection of rapamycin (0.04 mg/kg; MedChemExpress, HY-10219) on 0.5, 4.5 and 10.5 days, while the the control group was injected with saline of equal volume at the same days. Similarly, mice were killed on day 13.5. In addition to the recording of embryo implantation and resorption sites, the uterus was dissected to observe embryonic development, and fetal and placental weights were measured separately.

Statistical analyses

All analyses were conducted using GraphPad Prism 10.3 (GraphPad Software, CA, USA). Comparisons between two groups were performed using paired or unpaired Student's t-tests, Mann-Whitney U test, or Wilcoxon signed-rank test, based on normality and homogeneity of variance. Comparisons among multiple groups were performed using one-way or two-way ANOVA or Kruskal-Wallis test, depending on data distribution and variance homogeneity. All experiments were independently repeated at least three times. Data were presentedas mean ± SEM, and statistical significance was defined as $P < 0.05$.

Results

Increased senescence of DSCs in patients with RSA during early pregnancy

To explore the senescence status of DSCs during the development of RSA, we compared the expression differences of senescence-related markers in decidual tissues between normal pregnant women and RSA patients. Immunohistochemistry and immunofluorescence staining results showed that the expression of senescence-associated molecules CDKN2A/p16, CDKN1A/p21, and TP53/p53 were significantly elevated in DSCs of RSA patients (Fig. 1A and Figure S1A-B). Furthermore, senescence-associated beta-galactosidase (SA-β-gal) activity assays demonstrated that a substantially higher percentage of positive cells in the RSA group than that in the control group (Fig. 1B). These results indicate that there is abnormally enhanced cellular senescence in DSCs from RSA patients.

BCAAs trigger DSCs senescence by inducing oxidative stress

In our previous study, single-cell RNA sequencing (scRNA-seq) was used to compare DSCs from early pregnancy with endometrial stromal cells (ESCs) from the secretory phase. The results revealed that the expression levels of genes related to cellular senescence, BCAA transport, and oxidative stress increased in DSCs[19]. To clarify the effect of BCAA on the function of DSCs, we treated primary DSCs with exogenous BCAA and found that BCAA-induced cell senescence exhibited a significant time-dependent pattern (Fig. 2A). Further examination of senescence-associated molecules revealed that BCAA treatment significantly upregulated the expression of CDKN2A, CDKN1A, and TP53 (Fig. 2B). Consistent with these findings, SA-β-gal staining also confirmed that BCAAs caused a marked increase in the proportion of senescence-positive cells (Fig. 2C). Furthermore, given that oxidative stress is a an important inducer of cellular senescence, we evaluated the effect of BCAAs on intracellular reactive oxygen species (ROS) levels. Fluorescence probe assays revealed that BCAA treatment significantly promoted ROS production in DSCs (Fig. 2D). Collectively, these results indicate that excessive BCAA levels drive the senescence of DSCs by inducing intracellular oxidative stress.

BCAAs drive DSC senescence by suppressing autophagic activity

To elucidate the potential molecular mechanism underlying BCAAs-induced senescence in DSCs, we treated DSCs with media containing or lacking BCAA and then performed RNA sequencing (RNA-seq). The results revealed a total of 1121 differentially expressed genes (DEGs), of which 12 DEGs overlapped with the 288 known senescence-related genes (Fig. 3A-B). Subsequent KEGG pathway enrichment analysis revealed that these DEGs were predominantly involved in cellular senescence and autophagy pathways (Fig. 3C). Consistent with the sequencing data, RT-qPCR and western blot analyses confirmed

that BCAA treatment significantly downregulated the expression of key autophagy-related genes, including *ATG4B*, *ATG5*, *BECN1*, *MAP1LC3A*, and *MAP1LC3B* (Fig. 3D-E). Notably, autophagy inhibition by 3-methyladenine (3-MA) exacerbated cellular senescence (Fig. 3F-I). Conversely, rapamycin-mediated autophagy activation partially rescued D-galactose (D-Gal)-induced senescence (Fig. 3J). Together, these findings demonstrate that BCAAs promote DSC senescence through autophagy suppression.

Cellular senescence negatively regulates autophagic flux in DSCs

To investigate whether cellular senescence exerts feedback regulation on autophagy, we first established a senescence model in DSCs. Damage-induced senescence was triggered by exposing DSCs to H_2O_2, which led to a marked increase in senescence markers (CDKN2A, CDKN1A and TP53) (Fig. 4A-B). Notably, autophagic activity was markedly suppressed under these conditions, as reflected by downregulation of ATG5 and MAP1LC3B/LC3B, and concomitant accumulation of SQSTM1/p62 (Fig. 4C-D). To test the generality of this observation, D-galactose (30 mM) was used as an alternative senescence inducer. This treatment increased the SA-β-gal-positive rate and upregulated senescence-related proteins (Fig. 4E-F). Consistently, D-galactose-induced senescent DSCs also exhibited markedly impaired autophagic activity (Fig. 4G–H). Together, these findings establish that cellular senescence and autophagy reciprocally suppress each other, forming a negative feedback loop in DSCs.

Senescence negatively regulates FOXO1 expression in DSCs

Decidualization is crucial for the physiological function of DSCs and the maintenance of early pregnancy, and FOXO1 is a relatively classic decidualization-related molecule[20]. Bioinformatics analysis showed that differentially expressed genes (DEGs) were significantly enriched in cellular senescence and FOXO signaling pathways (Fig. 5A). Consistently, excessive BCAA exposure markedly diminished FOXO1 nuclear localization (Figure S2E) and protein levels in DSCs, as shown by immunofluorescence and western blot (Fig. 5B-C). FOXO1 expression was also significantly reduced in DSCs undergoing senescence induced by H_2O_2 or D-galactose (Fig. 5D-E and Figure S2A-B, S2F-G).

To further investigate the role of autophagy in regulating FOXO1, we similarly treated DSCs with the autophagy inhibitor 3-MA. The results showed that inhibiting autophagic flux led to a decrease in FOXO1 expression (Fig. 5F and Figure S2C, S2H). Conversely, activating of autophagy with rapamycin partially reversed the downregulation of FOXO1 expression induced by D-galactose (Fig. 5G). Crucially, clinical validation revealed that nuclear FOXO1 expression was significantly diminished in decidual tissues from patients with RSA compared to those from normal pregnancies (Fig. 5H-I). Together, these data suggest that impaired FOXO1 stability under conditions of high BCAA exposure or senescence is a critical factor leading to dysfunctional decidualization.

HSPA6 mediates senescence-associated DSC dysfunction through FOXO1 inhibition

To elucidate the specific molecular mechanisms underlying the regulation of FOXO1 expression during cellular senescence, we induced DSC senescence using D-galactose (30 mM) and then performed transcriptome sequencing (RNA-seq). Analysis of DEGs showed that there were a total of 160 DEGs in the control group and the D-Gal group, among which 82 were upregulated and 78 were downregulated (Fig. 6A). Based on the predicted network between DEGs and genes related to cell function, we found that heat shock protein family A member 6 (HSPA6) is closely associated with FOXO1 (Fig. 6B). As previously reported, HSPA6, an HSP70 family member, promotes trophoblast survival under oxidative stress via MMP2-mediated HBEGF shedding, with its dysregulation implicated in pregnancy complications[21]. In vitro experiments further demonstrated that HSPA6 was upregulated following senescence induction (Fig. 6C-F). Notably, HSPA6 knockdown significantly restored FOXO1 expression in DSCs (Fig. 6G–K). Clinically, HSPA6 was markedly elevated in decidual tissues from RSA patients (Fig. 6L-M). Together, these findings indicate that senescence suppresses FOXO1 via HSPA6 upregulation, thereby contributing to RSA pathogenesis.

High-dose leucine administration promotes adverse pregnancy outcomes via uterine senescence in mice

To clarify the impact of leucine on adverse pregnancy outcomes, we established a control group and a 6% high-leucine diet mouse model. As shown, on day 13.5 of pregnancy, the high leucine group exhibited a significant adverse pregnancy outcome (Fig. 7A). Although no significant difference was observed in the number of implants, the embryo absorption rate in the high leucine group was significantly increased, and the weight of embryos and placentas was reduced (Fig. 7B-D). In addition, the high-leucine diet led to enhanced SA-β-gal activity in the uterus, and the expression of senescence markers CDKN2A, CDKN1A and TP53 increased simultaneously (Fig. 7E-G and Figure S3A). Notably, we found that the autophagic flow in the uterus of mice in the high-leucine group was inhibited (Fig. 7H) and the expression of FOXO1 decreased (Fig. 7I and Figure S2D).

To further investigate the potential role of excessive senescence in abortion, we constructed another senescence mouse model by injecting D-galactose. The results confirmed that the expression of FOXO1 decreased in the D-galactose-induced senescence uterus (Fig. 7J). Finally, we verified that HSPA6 expression was elevated in the uterus of high-leucine-fed mice, which was highly consistent with the results of *in vitro* experiments. These data suggest that the aberrant accumulation of senescent DSCs increases the risk of spontaneous abortion.

Rapamycin inhibits excessive uterine senescence to improve pregnancy outcomes

To determine the potential value of autophagy intervention in DSC senescence as a treatment for spontaneous abortion, we administered a low dose of the autophagy inducer rapamycin for regular intraperitoneal injections. As expected, rapamycin intervention significantly reduced the risk of adverse pregnancy outcomes (Fig. 8A). Although the number of implantation sites showed no significant

difference, rapamycin effectively reversed the risk of embryo loss caused by high-leucine, and the weight of the embryo and placenta increased (Fig. 8B-D). Furthermore, rapamycin not only increased autophagic flux in the uterus of pregnant mice (Fig. 8E and Figure S3C), but also alleviated the state of excessive uterine senescence (Fig. 8F-G and Figure S3B). Thus, these findings demonstrate that rapamycin targets and enhances the autophagy level at the maternal-fetal interface, effectively inhibiting excessive uterine tissue senescence and subsequently reducing the risk of spontaneous abortion.

Discussion

BCAAs serve as crucial metabolic signaling molecules that play a central role in regulating cellular energy metabolism and protein synthesis; however, their metabolic dysregulation is closely associated with various pathophysiological processes[22–24]. In normal pregnancy, physiological levels of BCAAs at the maternal-fetal interface are indispensable for supporting embryonic development and ensuring successful decidualization[25, 26]. Interestingly, our study revealed that excessive accumulation of BCAAs induces DSC senescence, thereby disrupting metabolic homeostasis at the maternal-fetal interface. Previous studies have indicated that high concentrations of BCAA may not only induce mitochondrial dysfunction but also trigger the release of pro-inflammatory cytokines by continuously activating the mTORC1 signaling pathway[27]. Richardson et al.[28] demonstrated in a mouse model that restriction of BCAA intake significantly inhibited mTORC1 activity and alleviates age-related inflammation, revealing BCAA as a critical metabolic signal governing the core mechanisms of cellular senescence, thereby providing a strategic basis for managing pathological damage induced by metabolic disorders.

Autophagy as a core mechanism for cells to maintain protein homeostasis and intracellular environmental balance, plays a key role in resisting metabolic stress[29, 30]. In the field of reproduction, the blockade of autophagic flux is closely associated with various pregnancy complications, including recurrent miscarriage and preeclampsia[31, 32]. Notably, as a central nutrient sensor within cells, the activity of autophagic flux is strictly regulated by amino acid level[33]. In the present study, we found that aberrant accumulation of BCAAs led to significant autophagic flux blockage in DSCs. However, in the complex maternal-fetal interface metabolic network, it remains unclear how the fluctuations of BCAA interfere with the autophagy process and subsequently affect the fate determination of DSCs. Currently, the academic community generally believes that mTORC1 is the core hub for sensing BCAA levels[34]. High levels of BCAAs activate mTORC1, which subsequently phosphorylates ULK1 at specific sites (e.g., Ser 757), thereby disrupting the interaction between ULK1 and AMPK and ultimately suppressing autophagy initiation[35, 36]. Nevertheless, whether mTOR drives DSC senescence by directly regulating autophagosome-lysosome fusion or degradation processes, as well as its specific molecular targets in pregnancy failure, remains to be further investigated.

HSPA6, a member of the heat shock protein 70 (HSP70) family, has traditionally been recognized as a molecular chaperone under stress conditions, assisting in the refolding or targeted degradation of misfolded proteins through ATP-dependent mechanisms to maintain cellular protein homeostasis[37,

38]. However, recent studies have shown that HSPA6 can exhibit "double-edged sword" characteristics under pathological conditions. Specifically, it exerts a protective effect on cells during short-term stress, while continuous activation participates in the disease process through abnormal regulatory proteins[39, 40]. Interestingly, we found that persistent metabolic stress induced by BCAA leads to pathological accumulation of HSPA6 and accelerates decidual failure by targeting the degradation of FOXO1. This discovery reveals the non-classical function of the molecular chaperone system in pregnancy complications related to metabolic disorders.

FOXO1, as a master transcription factor for initiating and maintaining endometrial decidualization, its reduced activity directly impairs the functional maturation of DSCs and interferes with their normal communication with trophoblast cells[41, 42]. Previous studies have demonstrated that FOXO1 downregulation significantly diminishes its binding capacity to the promoter regions of target genes such as PRL and IGFBP1, while inducing aberrant activation of cell cycle regulatory genes (e.g., CDKN1A and CDKN1B/p27), thereby leading to defective decidual marker expression and impaired cell cycle arrest[43]. Consequently, the dysregulation of the HSPA6-FOXO1 axis emerges as a critical pathological mechanism underlying defective decidual development. Notably, our results show that HSPA6 knockdown partially restores FOXO1 protein levels and its transcriptional activity in DSCs. Nevertheless, the precise regulatory mechanisms by which cellular senescence modulates HSPA6, and whether additional metabolic pathways contribute to FOXO1 degradation, warrant further investigation.

Rapamycin, as a classic mTOR-specific inhibitor, has been proven to restore the self-cleaning ability of cells by alleviating mTORC1-mediated suppression of autophagy, and thereby significantly delay the senescence process of cells[44, 45]. Recent research has confirmed that rapamycin can improve ovarian aging in patients with endometriosis via the activation of the PPARα/IGFBP2 signaling pathway, thereby restoring fertility[46]. Importantly, Lu et al.[47] reported that low-dose rapamycin exhibited favorable safety profiles in animal models. In this study, administration of low-dose rapamycin exerted protective effects against spontaneous abortion in a high-leucine-induced senescence mouse model. Notably, however, rapamycin only partially rescued the leucine-induced blockade of autophagic flux, suggesting the involvement of mTOR-independent regulatory pathways. In additon, rapamycin exerts multiple effects, including reducing protein synthesis by inhibiting downstream effector molecules S6K1 and 4E-BP1 of mTORC1, regulating cell proliferation, inhibiting T/B cell activation to exert immunosuppression, activating mitochondrial autophagy, improving protein quality, and providing neuroprotection, etc. These pleiotropic mechanisms collectively lay the foundation for its widespread application in delaying aging and treating age-related diseases[48–50]. Consequently, a deeper understanding of how rapamycin precisely DSCs senescence through multidimensional pathways will facilitate the development of novel therapeutic targets and strategies for spontaneous abortion related to metabolic disorders.

Collectively, as shown in Fig. 9, elevated BCAA levels trigger excessive senescence in DSCs by inhibiting autophagic flux. This senescent state downregulates the expression of the key transcription factor FOXO1 in an HSPA6-dependent manner, thereby impairing decidual homeostasis and ultimately leading to spontaneous abortion. Notably, low-dose rapamycin intervention significantly alleviates cellular

senescence and improve pregnancy outcomes by activating autophagy. This study elucidates the crucial role of the “BCAA-autophagy suppression-cellular senescence-HSPA6-FoxO1” signaling axis in maintaining pregnancy, providing an important theoretical basis for metabolic intervention and clinical diagnosis and treatment of RSA.

Abbreviations

ATG4A: autophagy related 4A cysteine peptidase; ATG4B: autophagy related 4B cysteine peptidase; ATG5: autophagy related 5; BCAA: branched-Chain Amino Acid; BECN1: beclin 1; CDKN2A/p16: cyclin dependent kinase inhibitor 2A; CDKN1A/p21: cyclin dependent kinase inhibitor 1A; DEGs: differentially expressed genes; D-Gal: D-galactose; DSC: decidual stromal cell; FOXO1: forkhead box O1; GAPDH: glyceraldehyde-3-phosphate dehydrogenase; HSPA6: heat shock protein family A member 6; Leu: leucine; MAP1LC3A/LC3A: microtubule associated protein 1 light chain 3 alpha; MAP1LC3B/LC3B: microtubule associated protein 1 light chain 3 beta; mTOR: mechanistic target of rapamycin kinase; mTORC1: mechanistic target of rapamycin complex 1; NP: normal pregnancy; Rapa: rapamycin; ROS: reactive oxygen species; RSA: recurrent spontaneous abortion; SAβG: senescence-associated β-galactosidase; SASP: senescence-associated secretory phenotype; siHSPA6 DSCs: HSPA6-silenced DSCs; SQSTM1/p62: sequestosome 1; TP53/p53: tumor protein p53; 3-MA: 3-methyladenine

Declarations

Acknowledgments

We are grateful to the staff at Shanghai Genechem Co., Ltd. for their assistance with bioinformatics analysis.

Author Contributions

Hai-Xia Tan and Shao-Liang Yang contributed to investigation, visualization, writing the original draft. Jia-Wei Shi, Meng-Ying Li, Si-Man Chen, and Xiao-Yan Cao contributed to data curation and visualization. Wen-Jie Zhou, Ming-Qing Li, and Feng Xie contributed to methodology, supervision, reviewing and editing the manuscript, and visualization.

Funding Statement

This study was supported by the National Key Research and Development Program of China (2023YFC2705403), the National Natural Science Foundation of China (NSFC 82371673, 82301857, 32370914, 92478122, 92357306), the Shanghai Oriental Talent Plan, and the Shanghai Natural Science Foundation (17ZR1403200).

Availability of data and materials

The datasets involved in our study are available on reasonable request.

Ethics approval and consent to participate

The study protocol was approved by the Human Ethics Committee of the Obstetrics and Gynecology Hospital of Fudan University (approval No. 2023-136), and all participants provided written informed consent in accordance with the Declaration of Helsinki. All animal experiments were approved by the Animal Ethics Committee of the Obstetrics and Gynecology Hospital of Fudan University (approval No. 202311012S) and performed in accordance with the Guide for the Care and Use of Laboratory Animals.

Consent for publication

All authors agree to publish the content of the paper.

Competing interests

The authors declare that they have no competing interests.

References

1. Bender Atik R, Christiansen OB, Elson J et al (2023) Eshre guideline: recurrent pregnancy loss: an update in 2022. Hum Reprod Open 2023:hoad2. https://doi.org/10.1093/hropen/hoad002
2. Rai R, Regan L (2006) Recurrent miscarriage. Lancet 368:601–611. https://doi.org/10.1016/S0140-6736(06)69204-0
3. Dimitriadis E, Menkhorst E, Saito S et al (2020) Recurrent pregnancy loss. Nat Rev Dis Primers 6:98. https://doi.org/10.1038/s41572-020-00228-z
4. Jiang Y, Zhang Y, Li Y et al (2025) Research hotspots and trends in unexplained recurrent spontaneous abortion (ursa) from 2014 to 2024: a bibliometric analysis. Front Med (Lausanne) 12:1554875. https://doi.org/10.3389/fmed.2025.1554875
5. Muñoz-Espín D, Serrano M (2014) Cellular senescence: from physiology to pathology. Nat Rev Mol Cell Biol 15:482–496. https://doi.org/10.1038/nrm3823
6. Deryabin P, Griukova A, Nikolsky N et al (2020) The link between endometrial stromal cell senescence and decidualization in female fertility: the art of balance. Cell Mol Life Sci 77:1357–1370. https://doi.org/10.1007/s00018-019-03374-0
7. Yan Z, Zhou W, Ye J et al (2025) Cellular senescence in endometrium: a pivotal regulator in physiological remodeling and pathological disorders. Int J Biol Sci 21:6745–6758. https://doi.org/10.7150/ijbs.123036
8. Parvanov D, Ganeva R, Ruseva M et al (2026) Disrupted immune senescence in early pregnancy is associated with recurrent pregnancy loss. Front Immunol 17:1705823. https://doi.org/10.3389/fimmu.2026.1705823
9. Nonn O, Debnath O, Valdes DS et al (2025) Senescent syncytiotrophoblast secretion during early onset preeclampsia. Hypertension 82:787–799. https://doi.org/10.1161/HYPERTENSIONAHA.124.23362

10. Harrath AH, Rahman MA, Bhajan SK et al (2024) Autophagy and female fertility: mechanisms, clinical implications, and emerging therapies. Cells 13. https://doi.org/10.3390/cells13161354
11. Wan S, Huang Y, Yang H (2026) Shedding light on the function of autophagy in complicated pregnancies. Cell Death Dis 17:182. https://doi.org/10.1038/s41419-025-08311-7
12. Wang J, Tu S (2025) Stage-specific autophagy dynamics in reproductive processes and associated disorders. Front Cell Dev Biol 13:1639691. https://doi.org/10.3389/fcell.2025.1639691
13. Oestreich AK, Chadchan SB, Medvedeva A et al (2020) The autophagy protein, fip200 (rb1cc1) mediates progesterone responses governing uterine receptivity and decidualization†. Biol Reprod 102:843–851. https://doi.org/10.1093/biolre/ioz234
14. Tan H, Yang S, Li M et al (2020) Autophagy suppression of trophoblast cells induces pregnancy loss by activating decidual nk cytotoxicity and inhibiting trophoblast invasion. Cell Commun Signal 18:73. https://doi.org/10.1186/s12964-020-00579-w
15. Qin X, Shen H, Zhou W et al (2022) Insight of autophagy in spontaneous miscarriage. Int J Biol Sci 18:1150–1170. https://doi.org/10.7150/ijbs.68335
16. López AR, Frankel LB (2024) Selective degradation of ribosomes during oncogene-induced senescence: molecular insights and biological perspectives. Autophagy 20:1462–1464. https://doi.org/10.1080/15548627.2024.2319022
17. Bahar ME, Hwang JS, Lai TH et al (2026) The autophagy-senescence axis as a threshold model of aging and therapeutic targeting. Redox Biol 91:104079. https://doi.org/10.1016/j.redox.2026.104079
18. Wang X, Zhang L, Cao X et al (2025) The emerging roles of autophagy in the homeostasis of lysosome-related organelles. Front Cell Dev Biol 13:1638905. https://doi.org/10.3389/fcell.2025.1638905
19. Shi J, Lai Z, Zhou W et al (2024) Tnfsf14(+) natural killer cells prevent spontaneous abortion by restricting leucine-mediated decidual stromal cell senescence. Embo J 43:5018–5036. https://doi.org/10.1038/s44318-024-00220-3
20. Adiguzel D, Celik-Ozenci C (2021) Foxo1 is a cell-specific core transcription factor for endometrial remodeling and homeostasis during menstrual cycle and early pregnancy. Hum Reprod Update 27:570–583. https://doi.org/10.1093/humupd/dmaa060
21. Jain CV, Jessmon P, Barrak CT et al (2017) Trophoblast survival signaling during human placentation requires hsp70 activation of mmp2-mediated hbegf shedding. Cell Death Differ 24:1772–1783. https://doi.org/10.1038/cdd.2017.104
22. Li N, Li J, Wang H et al (2022) Branched-chain amino acids and their interactions with lipid metabolites for increased risk of gestational diabetes. J Clin Endocrinol Metab 107:e3058–e3065. https://doi.org/10.1210/clinem/dgac141
23. Bo T, Fujii J (2024) Primary roles of branched chain amino acids (bcaas) and their metabolism in physiology and metabolic disorders. Molecules 30. https://doi.org/10.3390/molecules30010056

24. Choi BH, Hyun S, Koo S (2024) The role of bcaa metabolism in metabolic health and disease. Exp Mol Med 56:1552–1559. https://doi.org/10.1038/s12276-024-01263-6
25. Jang C, Iosef C, Renaud SJ et al (2025) Amino acid restriction impairs human endometrial stromal cell decidualization and is rescued by proline supplementation. J Cell Mol Med 29:e70821. https://doi.org/10.1111/jcmm.70821
26. Bowman CE, Arany Z, Wolfgang MJ (2021) Regulation of maternal-fetal metabolic communication. Cell Mol Life Sci 78:1455–1486. https://doi.org/10.1007/s00018-020-03674-w
27. Ye Z, Wang S, Zhang C et al (2020) Coordinated modulation of energy metabolism and inflammation by branched-chain amino acids and fatty acids. Front Endocrinol (Lausanne) 11:617. https://doi.org/10.3389/fendo.2020.00617
28. Richardson NE, Konon EN, Schuster HS et al (2021) Lifelong restriction of dietary branched-chain amino acids has sex-specific benefits for frailty and lifespan in mice. Nat Aging 1:73–86. https://doi.org/10.1038/s43587-020-00006-2
29. Debnath J, Gammoh N, Ryan KM (2023) Autophagy and autophagy-related pathways in cancer. Nat Rev Mol Cell Biol 24:560–575. https://doi.org/10.1038/s41580-023-00585-z
30. Feng Y, Chen Y, Wu X et al (2024) Interplay of energy metabolism and autophagy. Autophagy 20:4–14. https://doi.org/10.1080/15548627.2023.2247300
31. Yang H, Lai Z, Shi J et al (2022) A defective lysophosphatidic acid-autophagy axis increases miscarriage risk by restricting decidual macrophage residence. Autophagy 18:2459–2480. https://doi.org/10.1080/15548627.2022.2039000
32. Huang Z, Cheng S, Jash S et al (2024) Exploiting sweet relief for preeclampsia by targeting autophagy-lysosomal machinery and proteinopathy. Exp Mol Med 56:1206–1220. https://doi.org/10.1038/s12276-024-01234-x
33. He R, Mo J, Lin Z et al (2026) The leucine-mtor-autophagy axis in granulosa cells mediates circadian disruption-induced anovulation. Int J Biol Sci 22:201–219. https://doi.org/10.7150/ijbs.116803
34. Wolfson RL, Chantranupong L, Saxton RA et al (2016) Sestrin2 is a leucine sensor for the mtorc1 pathway. Science 351:43–48. https://doi.org/10.1126/science.aab2674
35. Kim J, Kundu M, Viollet B et al (2011) Ampk and mtor regulate autophagy through direct phosphorylation of ulk1. Nat Cell Biol 13:132–141. https://doi.org/10.1038/ncb2152
36. Perveen R, Ozaki I, Takahashi H et al (2025) Bcaa (branched-chain amino acids) inhibiting the autophagy system via the activation of mtorc1, thereby upregulating the tumor suppressor pdcd4 in huh7 hepatoma cells. Cells 14. https://doi.org/10.3390/cells14241975
37. Fernández-Fernández MR, Gragera M, Ochoa-Ibarrola L et al (2017) Hsp70 - a master regulator in protein degradation. Febs Lett 591:2648–2660. https://doi.org/10.1002/1873-3468.12751
38. Rosenzweig R, Nillegoda NB, Mayer MP et al (2019) The hsp70 chaperone network. Nat Rev Mol Cell Biol 20:665–680. https://doi.org/10.1038/s41580-019-0133-3

39. Song B, Shen S, Fu S et al (2022) Hspa6 and its role in cancers and other diseases. Mol Biol Rep 49:10565–10577. https://doi.org/10.1007/s11033-022-07641-5
40. Zhu X, Chen X, Shen X et al (2024) Pp4r1 accelerates the malignant progression of nsclc via up-regulating hspa6 expression and hspa6-mediated er stress. Biochim Biophys Acta Mol Cell Res 1871:119588. https://doi.org/10.1016/j.bbamcr.2023.119588
41. Tanaka E, Koyanagi-Aoi M, Nakagawa S et al (2024) Effect of a foxo1 inhibitor on trophoblast differentiation from human pluripotent stem cells and erv-associated gene expression. Regen Ther 26:729–740. https://doi.org/10.1016/j.reth.2024.08.020
42. Wang M, Sun F, Zhang S et al (2024) Nek2 promotes the development of ovarian endometriosis and impairs decidualization by phosphorylating foxo1. Cell Mol Life Sci 81:237. https://doi.org/10.1007/s00018-024-05270-8
43. Guo Y, Tian W, Nie C et al (2026) Hbp1 enhances progesterone receptor activity and igfbp1 expression driving endometrial decidualization. Commun Biol 9:286. https://doi.org/10.1038/s42003-026-09567-1
44. Cayo A, Segovia R, Venturini W et al (2021) Mtor activity and autophagy in senescent cells, a complex partnership. Int J Mol Sci 22. https://doi.org/10.3390/ijms22158149
45. Panwar V, Singh A, Bhatt M et al (2023) Multifaceted role of mtor (mammalian target of rapamycin) signaling pathway in human health and disease. Signal Transduct Target Ther 8:375. https://doi.org/10.1038/s41392-023-01608-z
46. Wu Q, Fan J, Sheng Q et al (2026) Rapamycin improves endometriosis–related infertility involving ovarian senescence via the pparα/igfbp2 pathway. Mol Med Rep 33. https://doi.org/10.3892/mmr.2025.13722
47. Lu H, Yang H, Zhou W et al (2021) Rapamycin prevents spontaneous abortion by triggering decidual stromal cell autophagy-mediated nk cell residence. Autophagy 17:2511–2527. https://doi.org/10.1080/15548627.2020.1833515
48. Raghuvanshi K, Raghuvanshi D, Kumar D et al (2025) Exploring the role of mtor pathway in aging and age-related disorders. Excli J 24:992–1015. https://doi.org/10.17179/excli2025-8384
49. Ye L, Lee J, Xu L et al (2017) Mtor promotes antiviral humoral immunity by differentially regulating cd4 helper t cell and b cell responses. J Virol 91. https://doi.org/10.1128/JVI.01653-16
50. Chrienova Z, Nepovimova E, Kuca K (2021) The role of mtor in age-related diseases. J Enzyme Inhib Med Chem 36:1679–1693. https://doi.org/10.1080/14756366.2021.1955873

Figures

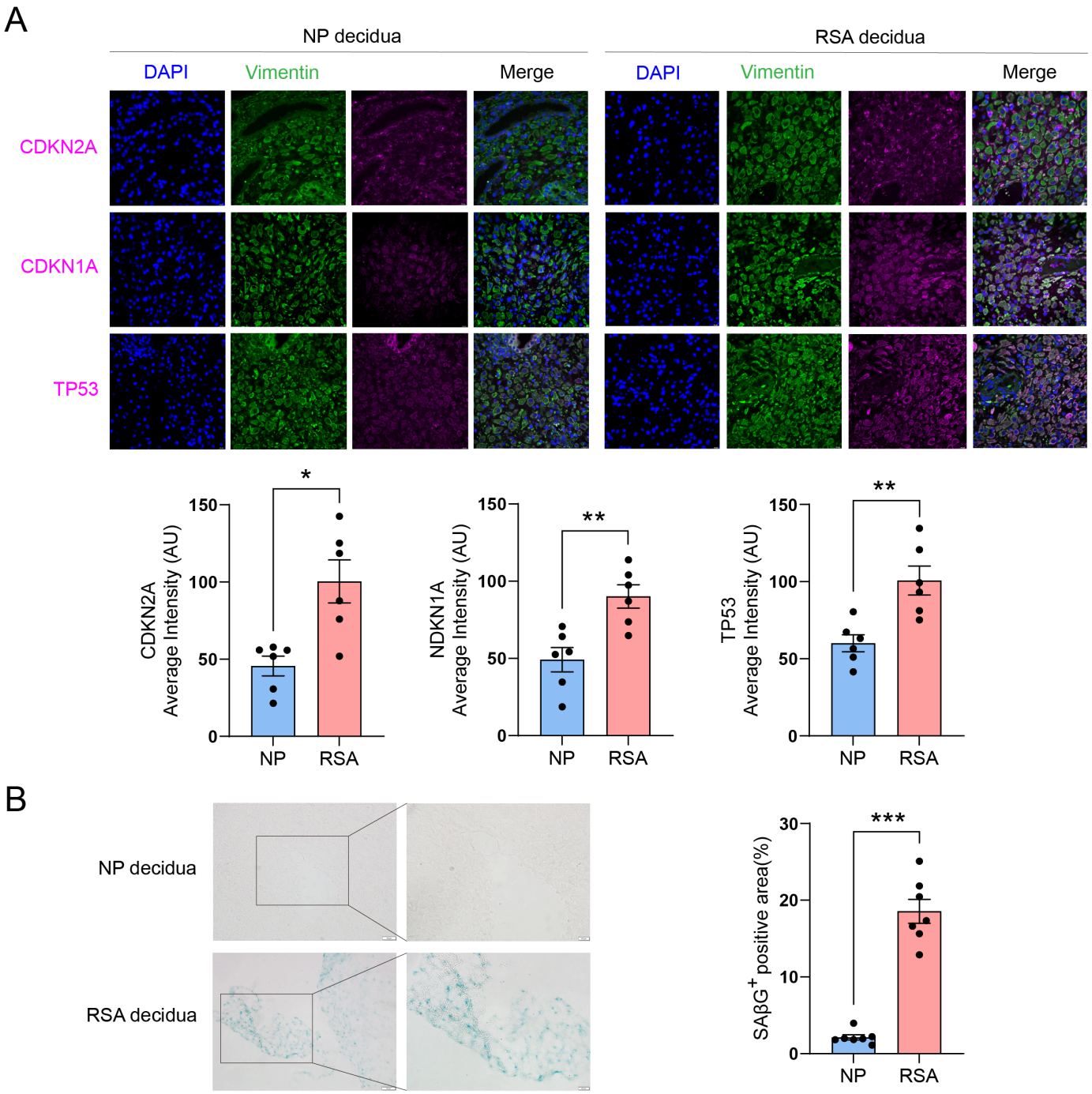


Figure 1

Increased senescence in DSCs from patients with RSA. (**A**) Immunofluorescence staining showed the expression of the above senescence-related proteins in DSCs in the normal group (n = 6) and RSA group (n = 6). Scale bar: 20 μm. (**B**) SA-β-gal staining was used to observe the proportion of senescent cells in decidual tissues from NP (n = 7) and RSA (n = 7). Scale bar: 50 μm and 20 μm. Data were presented as mean ± SEM and analyzed by unpaired t-test or Mann-Whitney U test. *P < 0.05, **P < 0.01, ***P < 0.001.

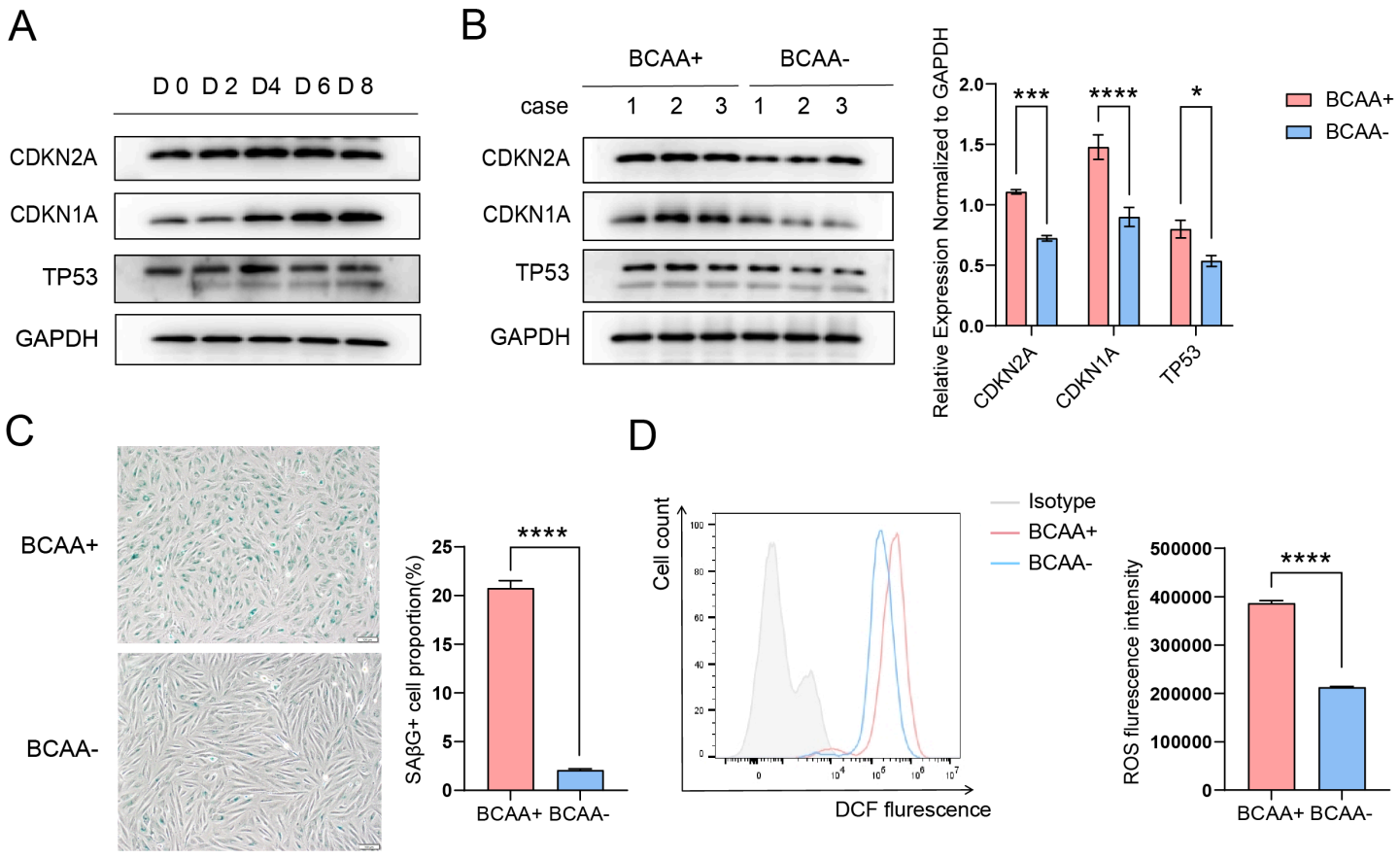


Figure 2

BCAAs trigger oxidative stress and cellular senescence in DSCs. (**A**) Western blot was used to detect the protein levels of senescence-associated molecules (CDKN2A , CDKN1A, and TP53) in DSCs treated with BCAAs at different time periods (0, 2, 4, 6, and 8 days). (**B**) DSCs were cultured in media with and without BCAA for 96 h, and the expression of DSC senescence-related molecules were detected by western blot (n = 3). The relative expression levels of proteins were normalized using the internal reference protein GAPDH. (**C**) SA-β-gal staining evaluated the effect of BCAA on DSC senescence, and the percentage of positive cells was statistically analyzed (n = 3). Scale bar, 100 μm. (**D**) DSCs were cultured in media with and without BCAA for 96 h, and intracellular ROS levels were subsequently measured by flow cytometry (n = 3). Data were presented as mean ± SEM and analyzed by two-way ANOVA test or unpaired t-test. *P < 0.05, ***P < 0.001, ****P < 0.0001.

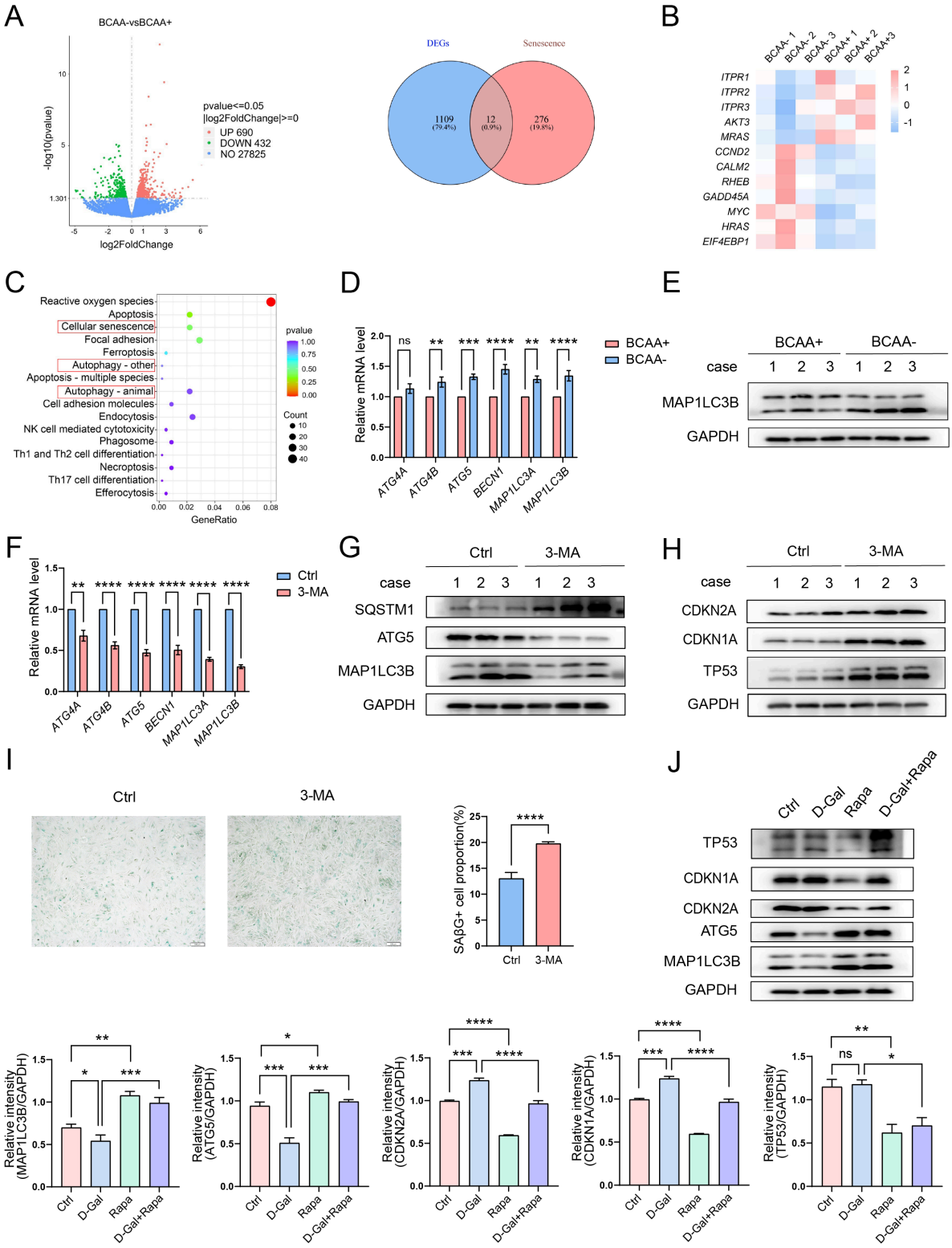


Figure 3

BCAAs drive DSC senescence by suppressing autophagic activity. (**A**) Volcano plot depicting DEGs in control (BCAA-, n = 3) versus BCAA-treated (BCAA+, n = 3) groups (left), with a Venn diagram showing overlap with senescence-associated genes (right). (**B**) Heatmap of DEGs related to senescence between BCAA- and BCAA+ groups. (**C**) KEGG pathway enrichment analysis of the DEGs. (**D**, **E**) The expression of autophagy-related genes and proteins in control (n = 3) versus BCAA-treated (n = 3) groupal staining

(left) and quantitative analysis (right) in control (n = 3) and 3-MA-treates were verified by qRT-PCR and immunoblot. (**F**, **G**) The inhibitory effect of 3-MA (10 mM) on autophagy was verified by qRT-PCR and immunoblot. (**H**) Immunoblot verified the expression of senescence-related proteins (CDKN2A, CDKN1A and TP53) in the control group (n = 3) and 3-MA group (n = 3). (**I**) SA-β-gd (n = 3) groups. Scale bar: 100 μm. (**J**) The expression of CDKN2A, CDKN1A, TP53, ATG5 and MAP1LC3B in the control group, D-Gal group, Rapa group, and D-Gal plus Rapa group were measured by immunoblot (n = 3). The relative expression levels of proteins were normalized using the internal reference protein GAPDH. Data were presented as mean ± SEM and analyzed by one-way ANOVA ,two-way ANOVA test, unpaired t-test or Mann-Whitney U test. *P < 0.05, **P < 0.01, ***P < 0.001, ****P < 0.0001, ns: no significance.

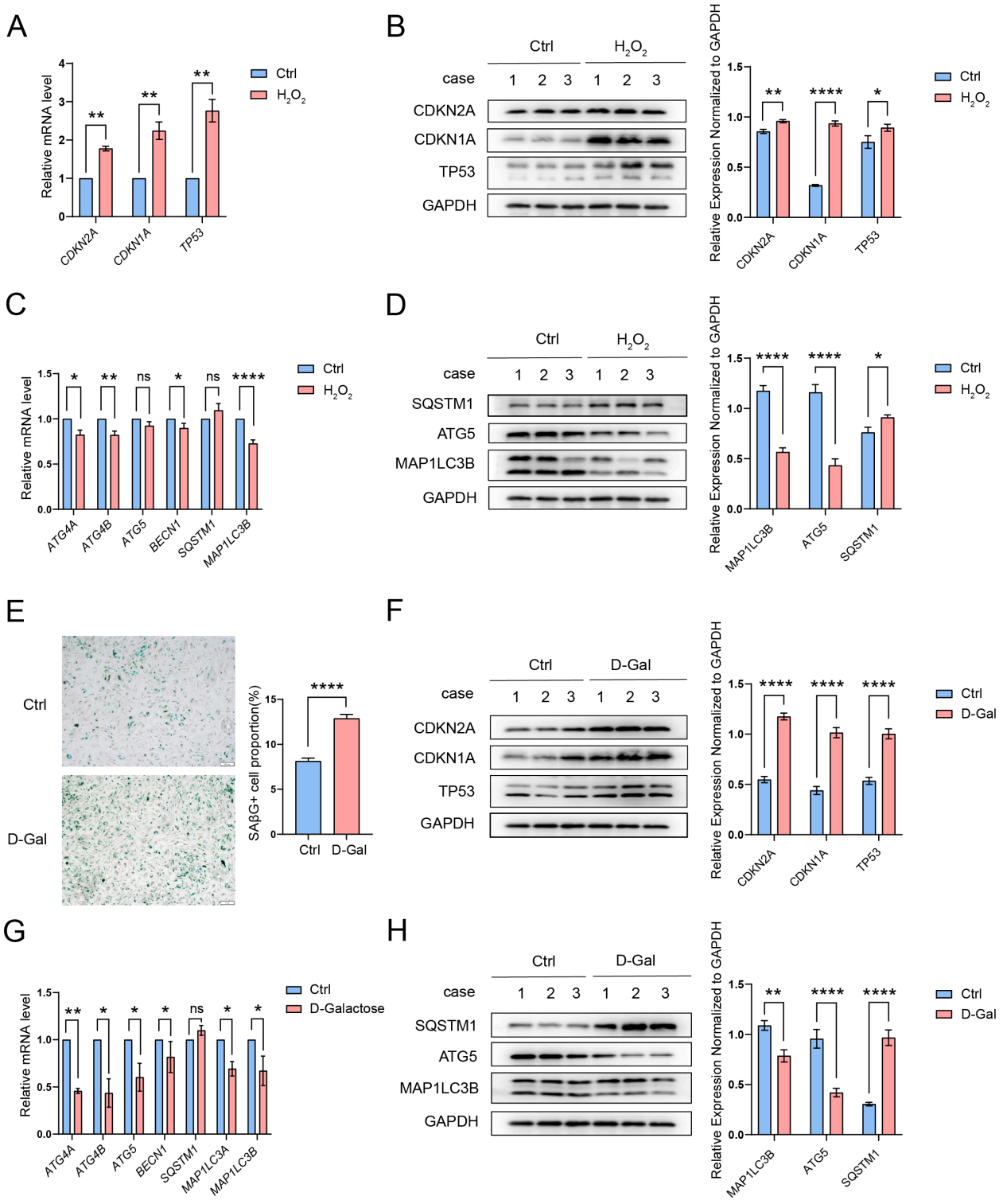


Figure 4

Senescence induction leads to decreased autophagy activity in DSCs. (**A**, **B**) The expression of senescence-associated genes and proteins in the control group (n = 3) and H_2O_2 group (n = 3) were detected by qRT-PCR and immunoblot. (**C**, **D**) qRT-PCR and immunoblot verified the expression of autophagy-related genes and proteins in the control group (n = 3) and H_2O_2 group (n = 3). (**E**) SA-β-gal staining and positive cell percentage in the control group (n = 3) and D-Gal group (n = 3). Scale bar, 100

μm. (**F**) Immunoblot detected the expression changes of autophagy-related proteins in DSC after D-galactose treatment (n = 3). (**G**, **H**) qRT-PCR and immunoblot verified the expression of autophagy-related genes and proteins in the control group (n = 3) and D-Gal (n = 3) group. Data were presented as mean ± SEM and analyzed by two-way ANOVA test, unpaired t-test or Mann-Whitney U test. *P < 0.05, **P < 0.01, ****P < 0.0001, ns: no significance.

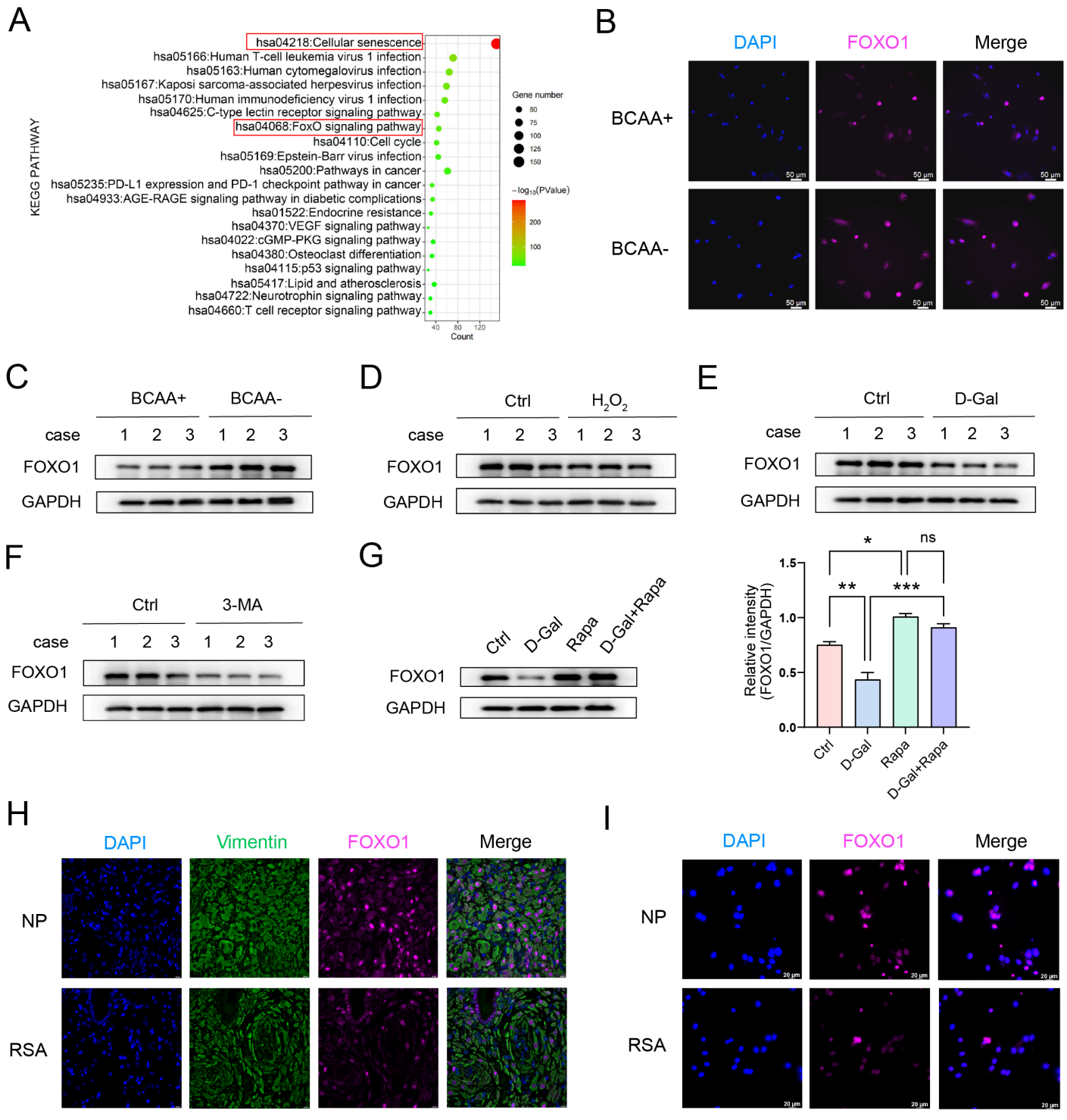


Figure 5

Senescence negatively regulates FOXO1 expression in DSCs. (**A**) KEGG pathway analysis of DEGs showed enrichment in cellular senescence and FOXO signaling pathways. (**B**, **C**) Immunofluorescence and immunoblot demonstrated the expression and nuclear localization of FOXO1 in DSCs under high BCAA treatment. Scale bar, 50 μm. (**D**, **E**) The protein expression of FOXO1 in senescent DSCs induced by H_2O_2 and D-galactose was detected by immunoblot (n = 3). The relative expression levels of proteins were normalized using the internal reference protein GAPDH. (**F**) Immunoblot analysis of FOXO1 levels in DSCs after treatment with the autophagy inhibitor 3-MA (10 mM) (n = 3). (**G**) Immunoblot showed that rapamycin (2 μM) partially rescued D-galactose-induced FOXO1 downregulation (n = 3). The relative expression levels of proteins were normalized using the internal reference protein GAPDH. (**H**-**I**) Nuclear expression of FOXO1 in decidual tissues and cells from normal pregnant patients (n = 6) and RSA patients (n = 6). Data were presented as mean ± SEM and analyzed by one-way ANOVA. *P < 0.05, **P < 0.01, ***P < 0.001, ns: no significance.

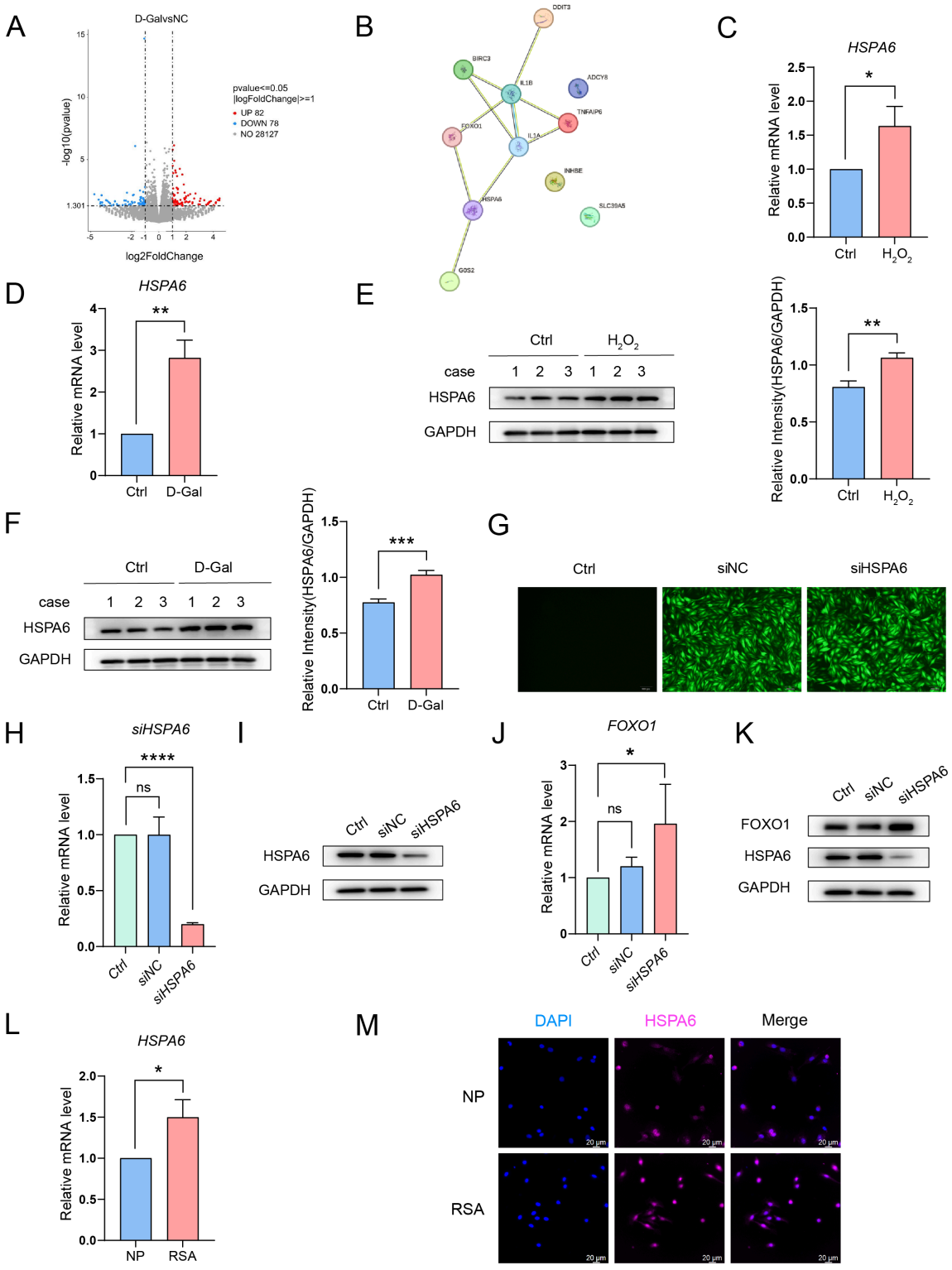


Figure 6

HSPA6 mediates senescence-associated DSC dysfunction through FOXO1 inhibition. (**A**) Volcano plots of DEGs in DSCs between the control group (n = 3) and the D-Gal group (n = 3). (**B**) Protein-protein interaction (PPI) network analysis based on transcriptome data revealed a close interaction relationship between HSPA6 and FOXO1. (**C**, **D**) The expression level of *HSPA6* mRNA in the control group (n = 6) and the H_2O_2 group (n = 6) or the D-Gal group (n = 6). (**E**, **F**) Immunoblot analysis of HSPA6 protein

expression in the control group (n = 3) and the H_2O_2 group (n = 3) or the D-Gal group (n = 3). The relative expression levels of proteins were normalized using the internal reference protein GAPDH. (**G**) Representative bright-field and fluorescence images of DSCs transduced with lentivirus carrying siNC or siHSPA6 after 72 h. Green fluorescent protein (GFP) expression indicates successful virus transduction. Scale bar, 100 μm. (**H**, **I**) Validation of *HSPA6* knockdown efficiency in DSCs at both mRNA (H) and protein (I) levels, respectively. (**J**, **K**) The *FOXO1* mRNA and protein expression levels after siHSPA6 were detected by RT-qPCR and immunoblot. (**L**) RT-qPCR analysis of *HSPA6* mRNA expression in decidual tissues from normal pregnancy (n = 9) and RSA patients (n = 9). (**M**) Immunofluorescence staining showed HSPA6 expression levels in DSCs from normal pregnancy (n = 6) and RSA patients (n = 6). Scale bar, 20 μm. Data were presented as mean ± SEM and analyzed by one-way ANOVA , unpaired t-test or Mann-Whitney U test. *P < 0.05, **P < 0.01, ***P < 0.001, ****P < 0.0001, ns: no significance.

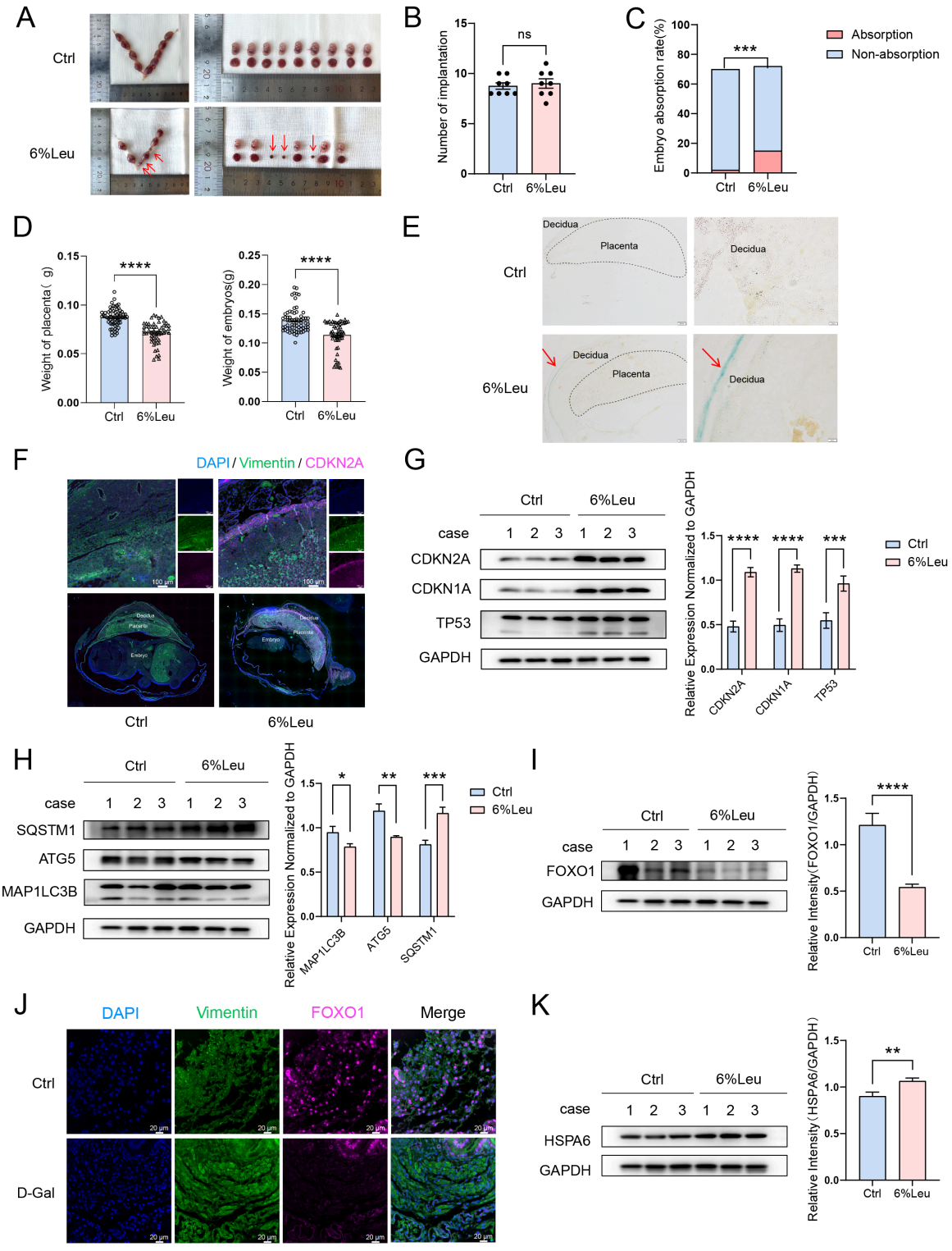


Figure 7

High-dose leucine administration promotes adverse pregnancy outcomes via uterine senescence in mice. (**A**) Photograph of mice uterus (red arrow: resorption point) and mice embryos and placentas. (**B**) The number of embryo implantations (Ctrl, n = 8; 6%Leu, n = 8). (**C**) Embryo absorption rate of control group and 6%Leu groups (Ctrl, n = 8; 6%Leu, n = 8). (**D**) The weight of placenta and embryo in both groups (Ctrl, n = 8; 6%Leu, n = 8). (**E**) SA-β-gal staining of uterine tissue sections showed an increase in

senescent cells induced by high leucine (n = 8). (**F**) Immunofluorescence detection of CDKN2A expression in DSCs of pregnant mice (Ctrl, n = 6; 6% Leu, n = 6). (**G**) Immunoblot detection of the expression of senescence markers CDKN2A, CDKN1A, and TP53 in uterine tissue (n = 3). The relative expression levels of proteins were normalized using the internal reference protein GAPDH. (**H**) Immunoblot detection of autophagic flux levels (MAP1LC3B, ATG5, SQSTM1) in uterine tissue (n = 3). (**I**) FOXO1 expression was verified by Immunoblot (n = 3). (**J**) Immunofluorescence analysis of FOXO1 expression in the uterus of D-galactose -induced senescence mouse models (n = 6). Scale bar: 20 μm. (**K**) HSPA6 expression level in uterine tissues was verified by immunoblot (n = 3). Data were presented as mean ± SEM and analyzed by two-way ANOVA test, unpaired t-test or Mann-Whitney U test. *P < 0.05，**P < 0.01，****P < 0.0001，ns: no significance.

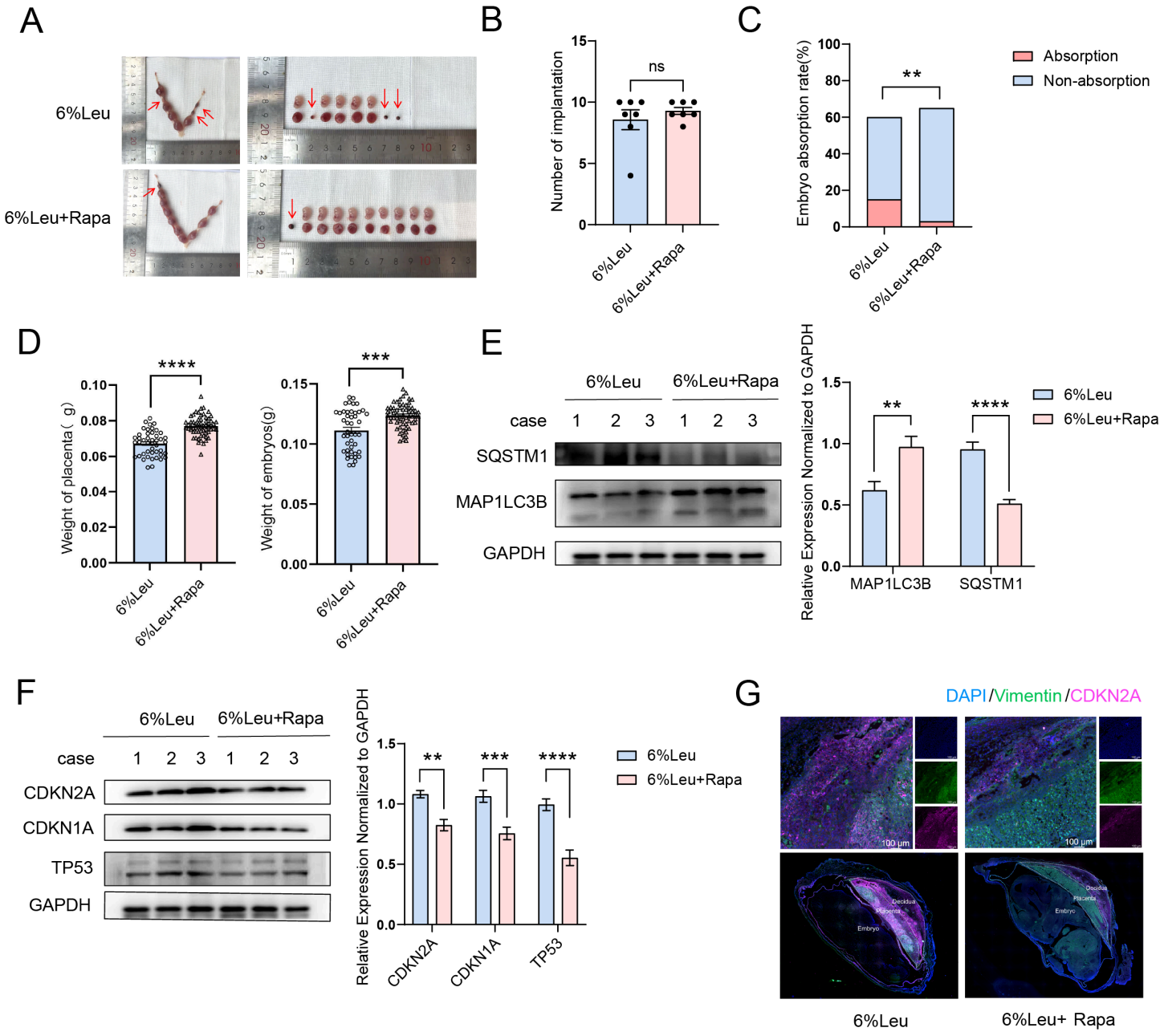


Figure 8

Rapamycin inhibits excessive uterine senescence to improve pregnancy outcomes. (**A**) Photograph of mice uterus (red arrow: resorption point) and mice embryos and placentas on day 13.5 of gestation. (**B**) The number of embryo implantations (6% Leu, n = 7; 6% Leu+Rapa, n = 7). (**C**) Embryo absorption rate in the 6% Leu and 6% Leu+Rapa groups (n = 7). (**D**) The weight of placenta and embryo in both groups (n = 7). (**E**) Immunoblott analysis of autophagy-related proteins (MAP1LC3B and SQSTM1) in uterine tissues to validate the activation of autophagic flux by rapamycin (n = 3). The relative expression levels of proteins were normalized using the internal reference protein GAPDH. (**F**) Immunoblot analysis of the expression of senescence markers CDKN2A, CDKN1A, and TP53 in uterine tissue. (**G**) Immunofluorescence detection of CDKN2A expression in DSCs of pregnant mice (6% Leu, n = 6; 6% Leu+Rapa, n = 6). Data were presented as mean ± SEM and analyzed by two-way ANOVA test, unpaired t-test or Mann-Whitney U test. **P < 0.01；***P < 0.001；****P < 0.0001；ns: no significance.

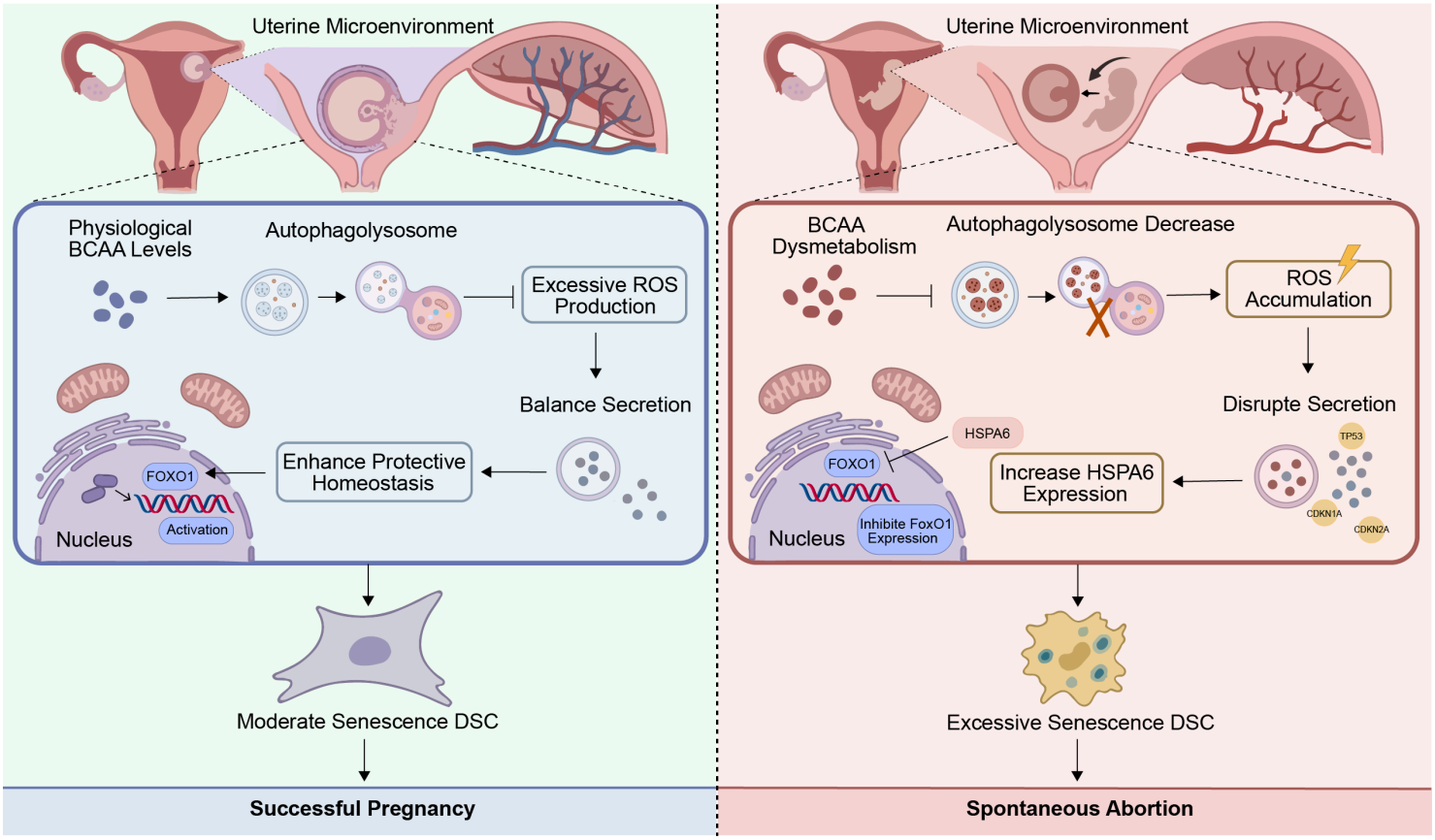


Figure 9

Schematic illustration of BCAA metabolism-autophagy axis in increasing spontaneous abortion risk by inducing excessive DSCs senescence. During normal pregnancy, physiological levels of BCAA metabolism maintain unimpaired autophagic flux and moderate ROS levels, activating the FOXO1 transcription program and promoting moderate senescence of DSCs to maintain the homeostasis of the uterine microenvironment. In contrast, during spontaneous abortion, BCAA metabolism disorder blocks autophagic flux, leading to ROS accumulation, upregulating senescence markers such as CDKN2A,

CDKN1A and TP53, inducing HSPA6 to enter the nucleus. Consequently, FOXO1 expression is suppressed, driving morphological transformations and excessive DSCs senescence, which ultimately leads to pregnancy failure through the disruption of decidual function.

Supplementary Files

This is a list of supplementary files associated with this preprint. Click to download.

- SupplementaryMaterial.docx